

Fast single image super-resolution based on sigmoid transformation

Longguang Wang, Zaiping Lin, Jinyan Gao, Xinpu Deng, Wei An¹

Abstract—Single image super-resolution aims to generate a high-resolution image from a single low-resolution image, which is of great significance in extensive applications. As an ill-posed problem, numerous methods have been proposed to reconstruct the missing image details based on exemplars or priors. In this paper, we propose a fast and simple single image super-resolution strategy utilizing patch-wise sigmoid transformation as an imposed sharpening regularization term in the reconstruction, which realizes amazing reconstruction performance. Extensive experiments compared with other state-of-the-art approaches demonstrate the superior effectiveness and efficiency of the proposed algorithm.

Index Terms—single image super-resolution, sigmoid transformation, sharpening regularization

I. Introduction

SUPER-resolution (SR) has been widely applied in video surveillance [1][2][8], remote sensing [3][4][5][35], medical imaging [6] [7] and many other fields, enhances the image resolution and provides pleasing image details, which is significant for subsequent image processing. Aiming to up-scale the image resolution based on single image [12], single image super-resolution (SISR) requires generating severalfold data from limited input data to approach natural images, which is badly ill-posed and often suffers from annoying blurring and artifacts.

To alleviate the ill-posed problem of SISR, many algorithms have been proposed to exploit additional information to learn how natural images are, which improves the reconstruction performance efficiently. Considering the difference between natural image information sources, the algorithms can be roughly subdivided into dictionary-based methods [9][17][18][33][34], self-exemplar-based methods [15][20][32] and prior-based methods [13][14][16]. Dictionary-based methods refer to external high resolution (HR) and corresponding low resolution (LR) image pairs as exemplars to hallucinate the missing details, which requires large scale databases to cover possible relationship between LR images and HR images. As external-exemplars-based methods are time-consuming in training procedure, self-exemplar-based methods assume redundancy of patches within the single image and utilize recurred local similar patches as exemplars to exploit underlying image details. Unlike dictionary-based and exemplar-based, prior-based methods utilize priors as constraints to alleviate the ill-posedness, perform robustly and

efficiently with no relying on exemplars.

Interpolation methods [22][23][26] as the simplest prior-based methods, utilize analytical interpolation formulae like bicubic scheme to predict new pixels based on local pixels, however the spline functions may not match natural images with strong discontinuities and lead to ringing artifacts along the edges. Smoothness prior [24][25] as another widely used category of image prior, regularizes the first or higher derivatives of the reconstructed image, suppressing the additional noises effectively but leading to transparent blurring. Recently sparsity deduced priors [14][21][27][28][31] have been extensively investigated which assume local image patch can be sparsely represented by linear combination of over-complete dictionary, however the sparsity assuming loses texture and other image details. To alleviate the blurring effect of edges in SISR, edge-based priors [11][13][16] are introduced to SISR and realize outstanding sharpening and deblurring effect. Fattal [11] proposed an edge deduced prior based on statistics of edge features, imposed the local continuity measures in the upscaled image to match the statistics learned from HR and LR image pairs. Sun [13][16] proposed a novel gradient profile prior, utilized 1-D profiles of gradient magnitudes to describe the gradient structure with a parametric gradient profile model learned from a large scale of natural images.

Considering upscaling leads to little degradation in flat region and dominant deterioration is mainly concentrated in edge and texture regions performing as blurring effect, we are motivated to utilize sharpening operation to alleviate the degradation with no relying on external exemplars. In this paper we propose an adaptive patch-wise sigmoid transformation to realize appropriate sharpening of the upscaled image, then utilize the sharpened image as an imposed regularization in the reconstruction and realize amazingly effective deblurring and sharpness enhancement. Different from [13][16] implementing the sharpening process in gradient space, our patch-wise method utilizes sigmoid function to match the slope of local intensities directly and steepens the slope with sigmoid transformation, which is similar to the image enhancement in [29][30]. With this simple but effective process, our method produces state-of-the-art SISR results with superior processing efficiency, and the reconstructed images are sharp and distinct with rare artifacts.

The reminder of this paper is organized as follow: In **Section II** we first introduce the patch-wise sigmoid transformation. Then in **Section III** we present the SISR framework based on sigmoid transformation. Extensive experiments are conducted comparing with state-of-the-art algorithms in **Section IV**. Finally the conclusions are drawn in **Section V**.

L. Wang is with the College of Electronic Science, National University of Defense Technology, Changsha, China. (wanglongguang15@nudt.edu.cn)

Z. Lin, J. Gao, X. Deng and W. An are also with the College of Electronic Science, National University of Defense Technology, Changsha, China.

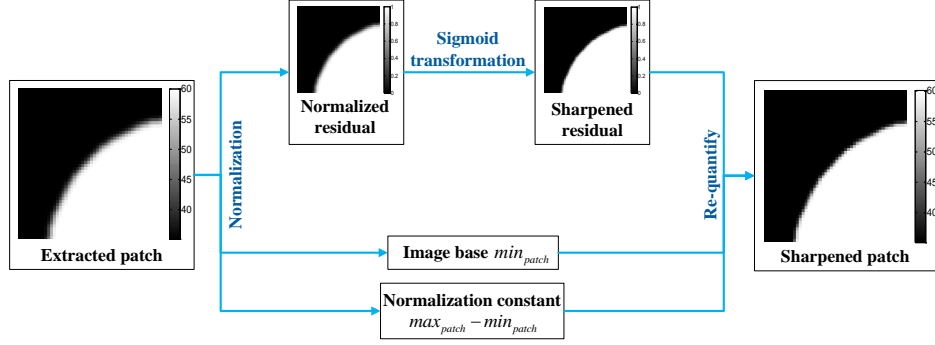


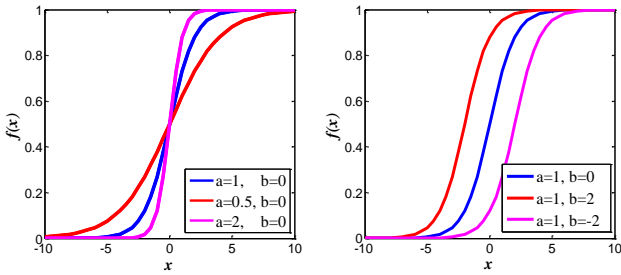
Fig.1 Overall sigmoid transformation.

II. PATCH-WISE SIGMOID TRANSFORMATION

In this section, the proposed patch-wise sigmoid transformation is presented and analyzed. We first formulate the sigmoid transformation, then perform parametrical analysis and finally compare our sharpening operation to other edge enhancement methods.

A. Formulation

In our scenario, the sharpening operation is implemented directly in image space instead of gradient space. Considering the continuity of natural images in local region, extracted local image patch can be regarded as a slope and the sharpening operation is equivalent to steepening the patch-wise slope intuitively. From the sketch of sigmoid function $f(x) = 1/(1 + \exp(-a(x + b)))$ shown in **Fig. 2**, we can see that sigmoid functions with varying parameter pairs a and b perform as superior characterizations of slopes with ranged steepness and location, therefore we are motivated to choose it as fitting function to characterize patch-wise slope, and the slope-based steepening can be realized through simple parametrical transformation.

Fig.2 Sketch of sigmoid functions with ranged parameter pairs a and b .

As shown in **Fig. 2**, the value of sigmoid function $f(x) = 1/(1 + \exp(-a(x + b)))$ ranges from 0 to 1, therefore the intensities within the patch need to be normalized first for subsequent sigmoid transformation.

$$y_{i,i \in patch} = \frac{z_i - \min_{j \in patch}\{z_j\}}{\max_{j \in patch}\{z_j\} - \min_{j \in patch}\{z_j\}}, \quad (1)$$

where z_i is the intensity of location i , y_i represents the normalized value, and $\min_{j \in patch}\{z_j\}, \max_{j \in patch}\{z_j\}$ refer to the minimum and maximum of the patch respectively. To avoid y_i equals to 0 or 1, we utilize a small constant ε set

to be 0.01 to fine-tune the maximum and minimum as

$$\begin{cases} \min_{j \in patch}\{z_j\} = \min_{j \in patch}\{z_j\} - \varepsilon \\ \max_{j \in patch}\{z_j\} = \max_{j \in patch}\{z_j\} + \varepsilon \end{cases} \quad (2)$$

With normalization operation implemented, sigmoid function $f_0(x) = 1/(1 + \exp(-a_0(x + b_0)))$ is introduced to fit the normalized residuals y_i to derive corresponding x_i values

$$y_i = f_0(x_i) \Rightarrow x_i = \frac{\ln(\frac{1}{y_i} - 1)}{-a_0} - b_0, \quad (3)$$

and then we transform x_i to sharpened residuals y'_i with sharpened sigmoid function $f_1(x) = 1/(1 + \exp(-a_1(x + b_1)))$

$$y'_i = f_1(x_i) = \frac{1}{1 + (\frac{1}{y_i} - 1)^{a_0} \cdot e^{a_1(b_0 - b_1)}} \quad (4)$$

Note that all intensities within the image patch are fused together for operation in this process, leading to strong robustness to noises and undulation.

Finally we re-quantify the sharpened residuals y'_i to derive sharpened intensities z'_i

$$z'_i = y'_i \times C_i + \min_{j \in patch}\{z_j\} \quad (5)$$

where $C_i = \max_{j \in patch}\{z_j\} - \min_{j \in patch}\{z_j\}$ represents the normalization constant.

As we can see from (4), the patch-wise sigmoid transformation can be regarded as a four-parameter problem, namely the sharpened image patch can be derived as parameters $\{a_0, a_1, b_0, b_1\}$ determined. Further observe (4), we can see it can be rewritten as

$$y'_i = \frac{1}{1 + (\frac{1}{y_i} - 1)^K \cdot e^B} = g(y_i; K, B)$$

$$\text{where } \begin{cases} K = \frac{a_1}{a_0} \\ B = a_1(b_0 - b_1) \end{cases} \quad (6)$$

Then the overall sigmoid transformation also degenerates into a two-parameter function as

$$z'_i = h(z_i; K, B) \quad (7)$$

where K determines the steepness of the sigmoid function while B determines the location, namely the non-symmetry of the sigmoid function. The overall process of sigmoid transformation is illustrated in **Fig. 1**.

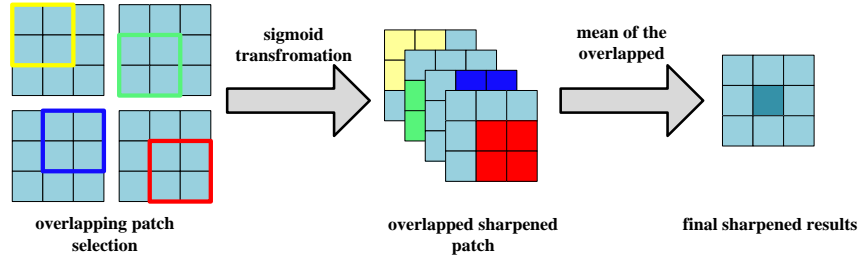


Fig.3 Overlapping strategy for patch-wise sigmoid transformation.

Considering patch-wise sigmoid transformation may generate block artifacts at the boundary between adjacent patches, we further utilize an overlapping strategy with Hanning window during implementation as shown in Fig. 3, and compute the mean value of overlapped pixels as the final sharpened results. As we can see, to implement the patch-wise sigmoid transformation with overlapping strategy, additional two parameters need to be determined, the size of image patch l_{patch} and the stride r_{patch} .

B. Parametrical analysis

As analyzed above, totally four parameters consisting of K, B, l_{patch} and r_{patch} need to be determined for sigmoid transformation. In this part, the parameters are analyzed respectively and empirically determined, while more experimental results are exhibited in Section V.

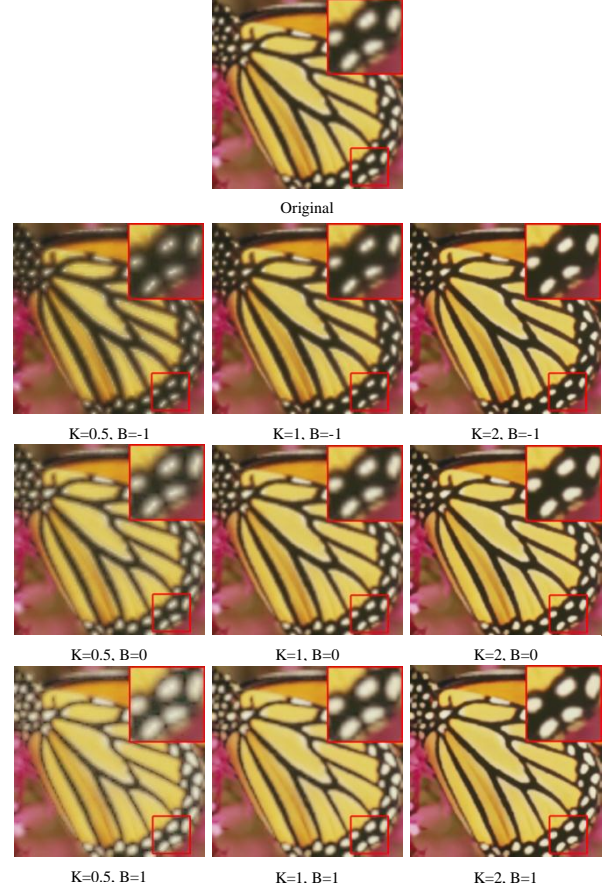
● Sharpness K

Remembering parameter K in (6) determines the steepness of the sigmoid function, it affects the sharpness and width of the edges directly. As we can see from left to right by row in Fig. 4, varying values of K lead to ranged sharpening effects, the larger K is, the sharper and narrower edges are. Moreover, it can be seen the sigmoid transformation performs as a blurring operation with smoothed and widened edges for $K < 1$, while performing as a sharpening operation with sharper and narrower edges for $K > 1$. Under the condition of $K = 1$, sigmoid transformation performs no sharpening or blurring with slope information well preserved in the results. Considering the requirement of image sharpening with computational cost, we empirically set $K = 2$ in this paper.

● Location B

Different with K , parameter B determines the location of the sigmoid function as shown in Fig. 2, namely affects the extension of the edges. After downsampling operation, some edges may not locate at the center of LR pixel, which is often the case especially when upscaling factor k is large. As shown in Fig. 4, we can see from top to bottom by column that the edges with varying values of B are displaced along the vertical direction, and the sign of B determines the direction. For $B < 0$ shown in the first row, the edges are displaced along the gradient direction, while displaced opposite to the gradient direction for $B > 0$ shown in the last row. Under the condition of $B = 0$, the edges are supposed to locate exactly at the center of pixel in LR image with no displacement during sharpening operation. Considering sub-pixel locations of edges in LR image vary between regions and are hard to estimate, especially when k is large,

therefore we empirically set $B = 0$ in this paper for simplicity.

Fig.4 Effects with ranged values of K and B . The results are derived from the blurred original image with different parameter settings.

● Patch size l_{patch} and stride r_{patch}

As a patch-wise slope-based sharpening operation, sigmoid transformation requires the patch size l_{patch} to cover complete slope information without disturbing information. Considering over-large patch size may introduce extra disturbing information and over small patch size may lose slope information, both leading to degradation of sharpening effect and generation of annoying artifacts, we empirically set $l_{patch} = 3$ in LR space to cover the neighboring information with little loss of slope information. To reduce the block artifacts at the boundary between patches, stride r_{patch} is required to cooperate with patch size l_{patch} to guarantee the compatibility between adjacent patches. Considering the computational cost, in this paper we empirically set

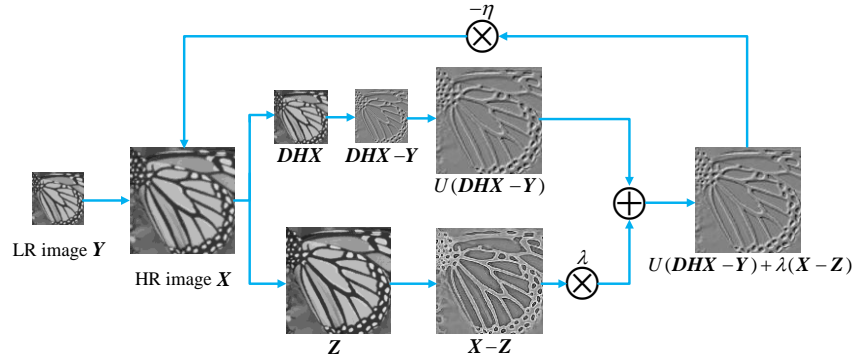


Fig.5 Overall SR framework.

$r_{patch} = 1$ in LR space for efficiency, namely $r_{patch} = k$ in HR space.

C. Relationship to other edge enhancement methods

As a generic edge-based prior for super-resolution, the proposed sigmoid transformation performs similarly with other edge enhancement methods. In this part, we discuss the relationship and inherent difference between the proposed sigmoid transformation and other representative edge enhancement methods.

Fattal [11] proposed an edge statistics prior for image up-scaling, namely edge-frame continuity modulus (EFCM), which is learned to characterize the marginal distribution of the gradients over the whole image. However, the imposed constrain on local continuity measures may not fit varying types of edges and generate jaggy artifacts, besides the computational cost is considerable as reported in [11].

Sun [13][16] establish a generic prior called gradient profile prior, and proposed gradient field transformation to transfer image gradient field guided by the prior knowledge learned from large training sets. However, the gradient profile only utilizes the pixel information along the gradient direction with local image structure neglected, leading to susceptibility to noises and undulation.

Shock filter is another representative category of edge enhancement approach, which is commonly designed to enhance edges detected by edge detectors. Recently, shock filter has been introduced into SR applications [] performing as an edge enhancement operation. However, as shock filter is sensitive to noise, the noise is supposed to be amplified while enhancing the edges.

Compared with other edge enhancement methods, the proposed sigmoid transformation performs twofold distinct differences or advantages. Firstly, the sigmoid transformation performs patch-wise and slope-based, namely the sharpening operation is based on local image structure, which is more reasonable with better suppression of noise. Secondly, our method performs superior efficiency, which is further demonstrated in Section IV.

III. SISR FRAMEWORK BASED ON SIGMOID TRANSFORMATION

In our scenario, the SISR process is realized through typical iterative reconstruction [21][27], where the patch-wise sigmoid transformation performs as an imposed sharpening

regularization cooperating with the reconstruction errors.

Given an HR image X and a corresponding LR image Y , the degradation process can be formulated as

$$Y = DHX + N \quad (8)$$

where H is the blurring operator, D determines the decimation matrix and N represents the additional Gaussian noise in Y . To realize the restoration of HR image X , we integrate the patch-wise sigmoid transformation as a sharpening regularization term with the reconstruction error in the cost function as

$$X = \operatorname{argmin}_X \{ \|DHX - Y\|^2 + \lambda \|X - Z\|^2 \} \quad (9)$$

where Z serves as a sharpened image of X utilizing the proposed patch-wise sigmoid transformation.

To solve the minimization problem in (9), we refer to our previous work in [] and utilize the fast upscaling technique in our SISR framework

$$X^{l+1} = X^l - \eta (U(DHX^l - Y) + \lambda (X^l - Z^l)) \quad (10)$$

where X^l , X^{l+1} are estimators of HR image X in l^{th} and $l+1^{th}$ iteration respectively, λ represents the regularization parameter weighting the regularization cost against the reconstruction error, η serves as the stepsize and $U(\cdot)$ refers to the upscaling technique proposed in [37].

The overall framework is shown in Fig. 5 and further summarized in algorithm 1.

Algorithm 1: SISR based on sigmoid transformation

Input: LR image Y , scaling factor γ

Initialize: Upscale the LR image Y utilizing interpolation method with bicubic spline to obtain original HR image X^0

Do:

- 1) Re-degenerate the HR image X^{l-1} and compute the reconstruction error $(DHX^{l-1} - Y)$, then utilize the upscaling technique [37] to upscale the reconstruction error;
- 2) Compute the sharpened image Z^{l-1} based on X^{l-1} utilizing the proposed patch-wise sigmoid transformation, then derive the difference between X^{l-1} and Z^{l-1} as a regularization term;
- 3) Update X^{l-1} to derive X^l according to (10).

Until: Stopping criteria are satisfied

Output: Reconstructed HR image X

IV. EXPERIMENTAL RESULTS

Implementation: As human vision is more sensitive to

brightness change, we only apply our method on brightness channel (Y) with color channels (UV) upscaled by bicubic interpolation for color images. In our experiments, the HR images are firstly blurred by a 7×7 Gaussian kernel with $\sigma = 1.2$, and then downsampled with factor $k = 3$ to serve as the input LR images. During the implementation of our method, regularization parameter λ and learning rate η are set to be 0.2 and 0.1 respectively, while the maximum num-

$$\left\{ \begin{array}{l} PSNR = 10 \log_{10} \left(\frac{255^2}{MSE} \right), MSE = \frac{1}{MN} \sum_{i=1}^M \sum_{j=1}^N (Y(i,j) - X(i,j))^2 \\ SSIM = \frac{(2\mu_x\mu_y + c_1)(2\sigma_x\sigma_y + c_2)}{(\mu_x^2 + \mu_y^2 + c_1)(\sigma_x^2 + \sigma_y^2 + c_2)}, \left\{ \begin{array}{l} c_1 = (k_1 L)^2 \\ c_2 = (k_2 L)^2 \end{array} \right. \end{array} \right. \quad (11)$$

where μ_x, μ_y are mean value of image X and Y respectively, σ_x, σ_y are standard variance of X and Y respectively, c_1, c_2 are two stabilizing constants with L representing the dynamics of a pixel value, and k_1, k_2 are generally set to be 0.01 and 0.03 respectively.

A. Experimental analysis of parameters

In this section, we focus on the sharpness parameter K and location parameter B , conduct extensive experiments on **Set5** and **Set14** datasets to test the effects of our method with various parameter settings.

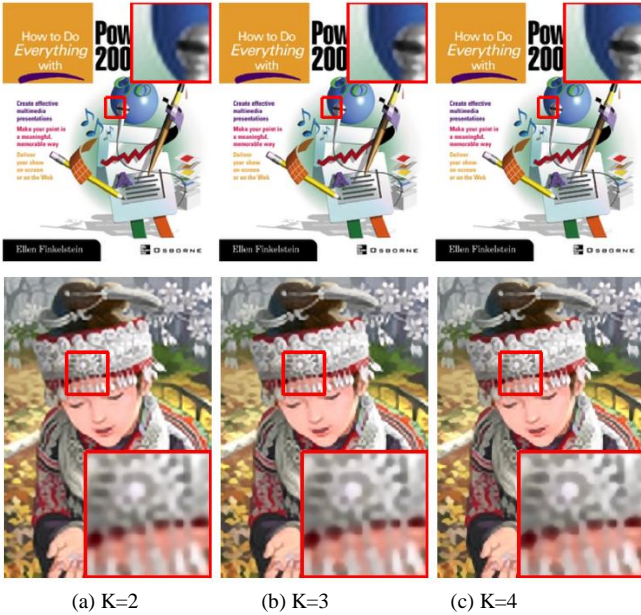


Fig.6 Effect of parameter K on image *PPT* and *Comic*. The images are reconstruction results (3X) with $K = 2, 3, 4$.

Fig. 6 presents the effects of sharpness parameter K on the reconstruction result. As we can see, larger K leads to sharper and narrower edges, however, over-sharp artifacts can be visible when K is over-large.

In **Fig. 7**, effects of location parameter B on the reconstruction result is given. Zooming in on the images, the displacement of edges can be observed between the results with different values of B . Compare the enlarged region of *Lenna*, the widening of the brown region under *Lenna*'s hat with B increased can be noticeable.

ber of iterations specified as 30.

All the experiments are coded in Matlab R2011 and running on a workstation with Septuple Core i7 @ 3.60 GHz CPUs and 16GB RAM.

Metrics: To evaluate and compare the results quantitatively, peak-signal-to-noise ratio (PSNR) and mean structure similarity (SSIM) are utilized as metrics, which are defined as

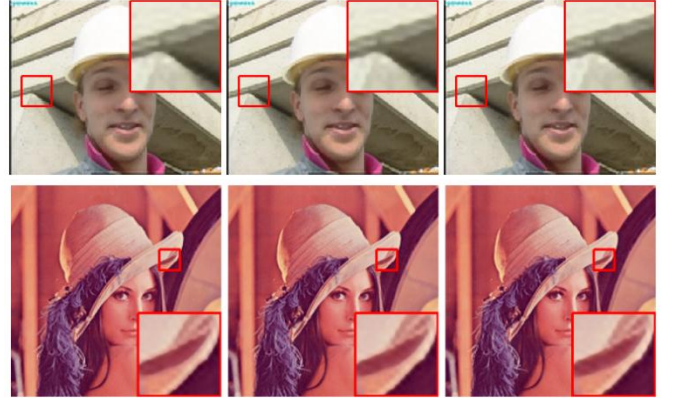


Fig.7 Effect of parameter B on image *Foreman* and *Lenna*. The images are reconstruction results (3X) with $B = -1, 0, 1$.

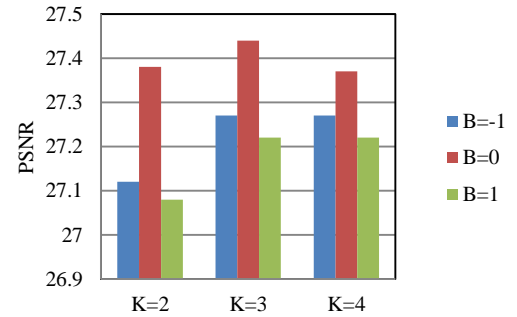


Fig.8 Average PSNR of different parameter settings.

Comparison of quantitative performance is exhibited in **Table. I** with average performance presented in **Fig. 8**. As sharpness parameter K increases, the reconstruction performance is first improved and then begins to deteriorate due to the over-sharp effects. Concerning location parameter B , obviously it has great impacts on the performance with $B = 0$ performing as the dominant one. However, note that it does not mean no benefits of B in fine-tuning the locations of edges, which can be validated by some superior results in **Table. I** with $B \neq 0$. As edges within an image varies remarkably, the fine-tuning is required to implement adaptively, nevertheless, the global selection of B and implementation of fine-tuning in our scenario may not adapt to most edges, commonly leading to degeneration of reconstruction performance.

Note that the adaptive selection of K and B is not the

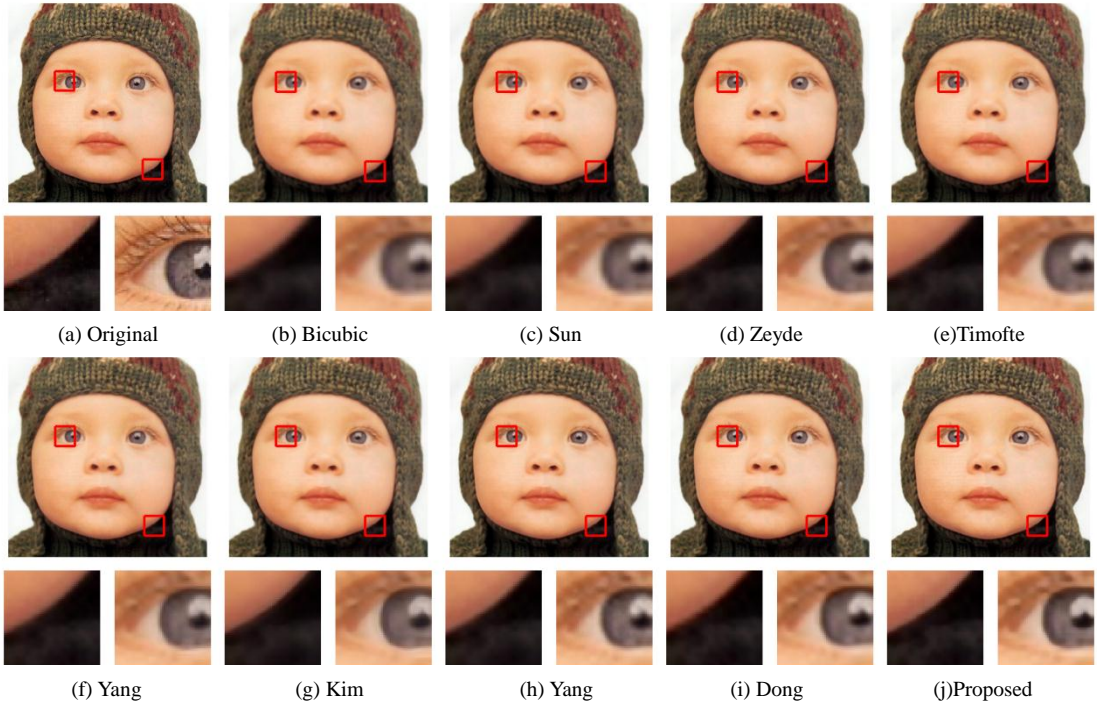
Fig.9 SISR results (3X) on image *Baby* by ranged methods.

TABLE I COMPARISON OF PSNR WITH DIFFERENT PARAMETER SETTINGS. THE BEST RESULT ARE SHOWN IN BOLD.

	$K = 2$			$K = 3$			$K = 4$		
	$B = -1$	$B = 0$	$B = 1$	$B = -1$	$B = 0$	$B = 1$	$B = -1$	$B = 0$	$B = 1$
Baby	33.00	33.22	32.93	32.92	33.04	32.87	32.72	32.79	32.69
Bird	30.83	31.19	30.96	30.85	31.08	30.94	30.73	30.88	30.78
Butterfly	23.97	24.75	24.02	24.68	25.21	24.67	24.90	25.25	24.88
Head	30.37	30.41	30.32	30.36	30.36	30.29	30.30	30.30	30.24
Woman	28.70	28.79	27.99	28.94	28.90	28.26	28.88	28.78	28.31
Baboon	21.28	21.32	21.31	21.27	21.30	21.29	21.25	21.27	21.27
Barbara	25.09	25.14	25.05	25.09	25.12	25.06	25.06	25.07	25.03
Coastguard	25.56	25.73	25.70	25.60	25.75	25.75	25.60	25.73	25.75
Comic	22.22	22.33	22.08	22.35	22.38	22.18	22.35	22.34	22.19
Flowers	25.70	25.98	25.80	25.84	26.04	25.92	25.86	26.00	25.92
Foreman	31.05	31.11	30.20	31.35	31.28	30.56	31.37	31.25	30.66
Lena	30.34	30.63	30.49	30.39	30.58	30.50	30.33	30.46	30.42
Monarch	29.17	29.75	29.12	29.68	30.05	29.57	29.80	30.03	29.68
Pepper	30.29	30.48	30.18	30.38	30.48	30.26	30.34	30.38	30.23
PPT	23.00	23.45	23.27	23.30	23.63	23.53	23.41	23.64	23.59
Zebra	26.37	27.07	26.79	26.58	27.11	27.02	26.56	26.95	26.95
Bridge	24.84	24.99	24.90	24.88	24.99	24.94	24.87	24.94	24.92
Man	26.30	26.49	26.28	26.42	26.55	26.40	26.44	26.52	26.41
Average	27.12	27.38	27.08	27.27	27.44	27.22	27.27	27.37	27.22

focus of this paper, we empirically set $K = 2$ and $B = 0$ for following experiments and leave this problem for further investigation.

B. Comparison to other methods

In this section, experiments are conducted on Set5 and Set14 datasets to compare the reconstruction performance of other state-of-the-art approaches, including bicubic, Kim *et al.*'s method [14], Zeyde *et al.*'s method [31], Timofte *et al.*'s method [18] and Yang *et al.*'s method [28], Dong *et al.*'s method [36], Sun *et al.*'s method [16] and Yang *et al.*'s method [17]. The source codes of approaches [14][31][18][28][17][36] are downloaded from the authors' homepages, and we refer to Yang's implementation work in [19] to derive other approaches [10][13][16] for no available originally released codes. Recommended parameters of comparing methods by the authors are used in our experiments.

We summarize the parameter settings for our method in Table II, and the reconstruction results are exhibited in Figs.

9-13 with quantitative results presented in Table III.

TABLE II PARAMETER SETTINGS FOR THE PROPOSED METHOD.

Parameters	Values
Sharpness K	2
Location B	0
Patch size l_{patch}	3 (in LR space)
stride r_{patch}	1 (in LR space)

• Visual quality

From the reconstruction results on image *Baby*, *Butterfly*, *Head*, *Comic* and *Lena* with upscaling factor 3 shown in Figs. 9-13, we can see that the bicubic interpolation method blurs the edge and texture regions remarkably with a serious loss of image details. Sun's method generates sharper edges, however the blurring effect is still noticeable. For Zeyde's method, Timofte's method, Yang's method and Yang's method, the blurring effect is further alleviated, but some ringing artifacts around the edges can still be visible. Relying on adaptive sparse representation, Dong's method achieves relatively

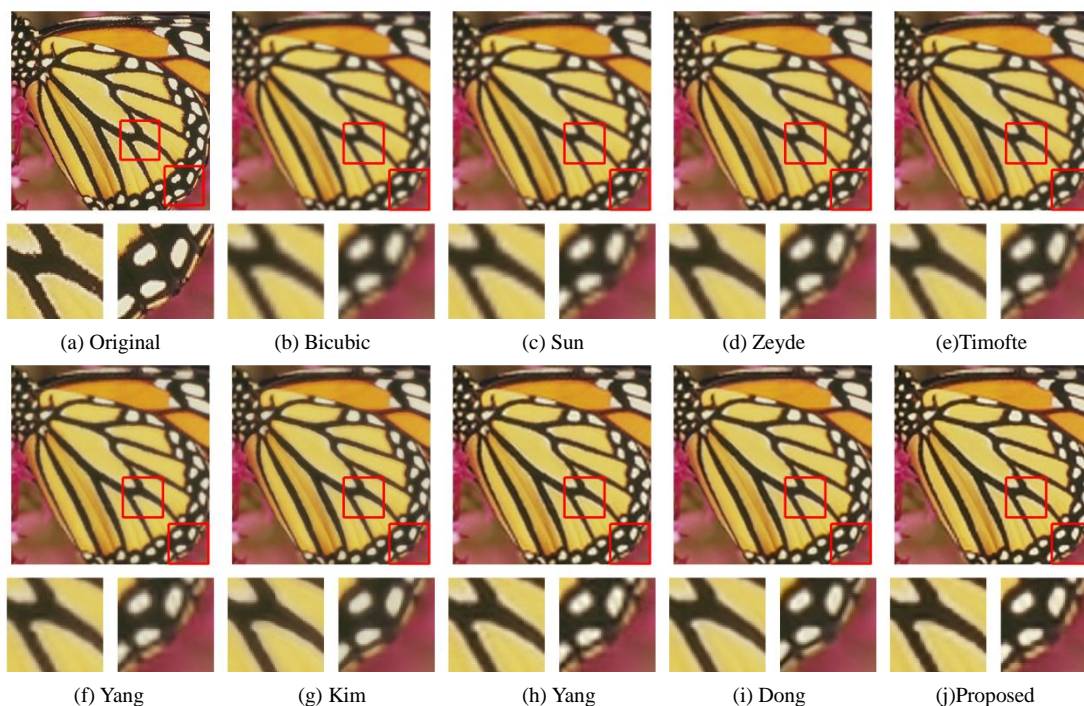


Fig.10 SISR results (3X) on image *Butterfly* by ranged methods.



Fig.11 SISR results (3X) on image *Comic* by ranged methods.

excellent visual quality, however some fine details like texture are missed due to the sparsity regularization. Kim's method generates sharp edges and distinct details, performs superior reconstruction performance. Concerning our proposed method, comparable top visual quality is achieved with even more fine details reconstructed, demonstrating the superiority of our proposed method.

● Quantitative metrics

As we can see in **Table. III**, the proposed method outper-

forms other approaches on all the test images with highest PSNR and SSIM values. Compared with Sun's method, our method performs remarkable improvement with PSNR value improved by 1.61 dB in average. Concerning state-of-the-art Kim's and Yang's method, the proposed method improves the average PSNR value with about 0.7 and 0.3 dB respectively, demonstrating the superior reconstruction performance of the proposed method.



Fig.12 SISR results (3X) on image *Lena* by ranged methods.

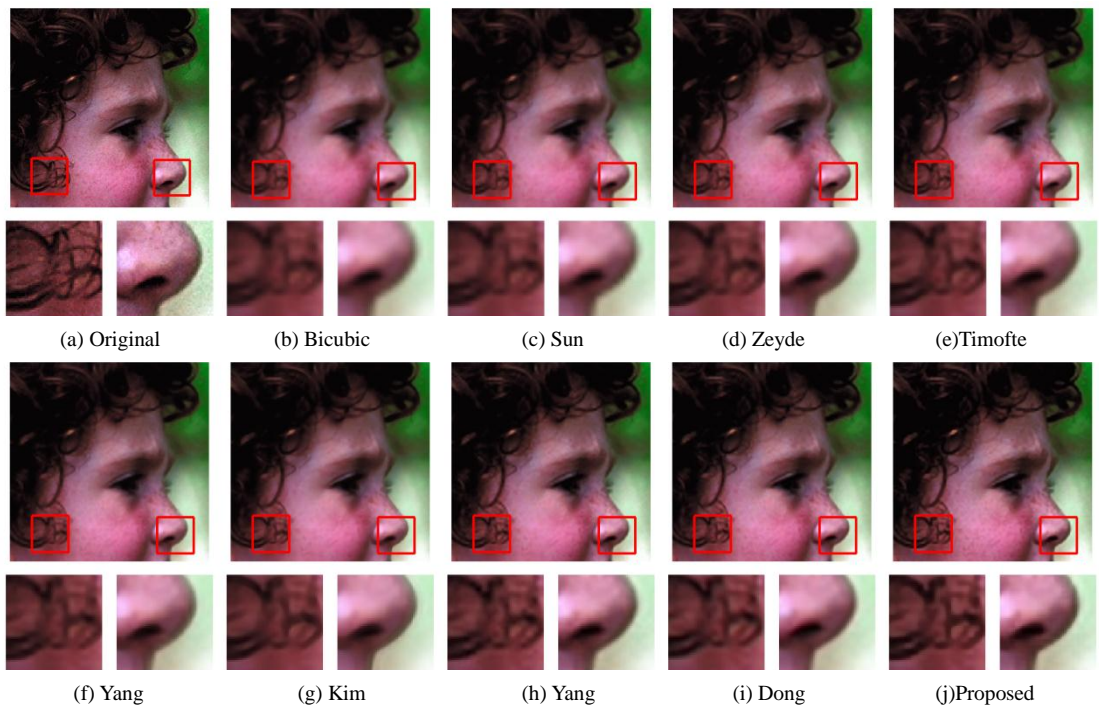


Fig.13 SISR results (3X) on image *Head* by ranged methods.

● Running time

In terms of processing efficiency, obviously the running time of bicubic interpolation method is much faster for no complex calculations. Some dictionary-based methods like Zeyde's, Timofte's and Yang's methods also performs superior

or efficiency, however note that the learning processes of these methods are hugely time-consuming. Concerning our proposed method, there is no need for additional training process and the running time is still faster than Kim's, Yang's, Yang's, Dong's and Sun's methods, even comparable to

TABLE III COMPARISON OF PSNR, SSIM AND RUNNING TIME. THE BEST RESULT ARE SHOWN IN BOLD.

	Metrics	Bicubic	Sun [16]	Zeyde [31]	Timofte [18]	Yang [28]	Kim [14]	Yang [17]	Dong [36]	Proposed
Baby	PSNR	30.91	31.47	32.12	32.11	32.11	32.22	32.86	28.32	33.22
	SSIM	0.848	0.861	0.871	0.873	0.874	0.875	0.886	0.825	0.895
	Time	0.011	59.354	2.779	0.804	192.766	18.172	7.740	400.262	5.165

Bird	PSNR	28.72	29.29	30.06	30.06	30.00	30.29	30.89	26.26	31.19
	SSIM	0.870	0.882	0.894	0.896	0.895	0.899	0.903	0.815	0.904
	Time	0.005	14.287	1.172	0.526	56.172	9.271	3.558	122.515	1.902
Butterfly	PSNR	21.33	21.95	22.93	22.86	22.96	23.76	23.88	20.23	24.75
	SSIM	0.742	0.769	0.815	0.810	0.817	0.846	0.835	0.759	0.849
	Time	0.005	10.342	0.935	0.543	42.526	18.601	2.844	134.362	1.663
Head	PSNR	29.43	29.67	29.95	30.00	30.00	30.08	30.25	28.08	30.41
	SSIM	0.692	0.703	0.714	0.717	0.718	0.718	0.727	0.670	0.741
	Time	0.005	14.094	1.033	0.473	55.657	50.75	2.889	109.330	1.829
Woman	PSNR	25.66	26.24	27.24	27.20	27.22	27.56	28.33	23.46	28.79
	SSIM	0.840	0.855	0.874	0.875	0.875	0.879	0.892	0.817	0.899
	Time	0.005	13.434	1.112	0.449	53.079	9.756	3.080	119.914	1.776
Baboon	PSNR	20.75	20.89	21.03	21.08	21.09	21.13	21.24	20.37	21.32
	SSIM	0.423	0.441	0.457	0.464	0.468	0.470	0.490	0.423	0.512
	Time	0.010	72.780	2.641	0.834	165.652	26.970	9.861	398.111	4.460
Barbara	PSNR	24.04	24.27	24.89	24.60	24.63	24.68	24.90	22.86	25.14
	SSIM	0.678	0.692	0.710	0.712	0.714	0.715	0.729	0.652	0.743
	Time	0.014	116.127	4.622	1.161	297.839	33.783	15.519	699.157	7.505
Coastguard	PSNR	24.60	24.85	25.26	25.21	25.35	25.34	25.54	23.93	25.73
	SSIM	0.527	0.548	0.569	0.574	0.582	0.577	0.596	0.518	0.627
	Time	0.006	23.299	1.241	0.547	70.530	12.450	3.957	156.050	2.121
Comic	PSNR	20.73	21.05	21.49	21.57	21.62	21.76	22.04	19.72	22.33
	SSIM	0.615	0.640	0.672	0.677	0.682	0.689	0.707	0.596	0.731
	Time	0.005	16.556	1.210	0.471	64.117	14.991	4.115	162.344	1.978
Flowers	PSNR	24.25	24.62	25.15	25.18	25.21	25.35	25.68	22.96	25.98
	SSIM	0.728	0.743	0.760	0.762	0.764	0.766	0.774	0.696	0.782
	Time	0.008	36.631	2.259	0.799	131.354	22.832	6.917	289.215	3.458
Foreman	PSNR	28.23	28.81	29.75	29.71	29.63	30.30	30.82	27.11	31.11
	SSIM	0.863	0.874	0.889	0.830	0.891	0.898	0.902	0.860	0.906
	Time	0.008	18.407	1.242	0.495	67.332	9.451	3.659	158.952	2.101
Lena	PSNR	28.81	29.23	29.84	29.86	29.88	30.14	30.49	26.45	30.63
	SSIM	0.755	0.766	0.777	0.779	0.780	0.783	0.790	0.726	0.797
	Time	0.010	55.387	2.790	0.827	192.144	17.336	8.212	410.589	5.184
Monarch	PSNR	26.63	27.22	28.07	28.04	28.10	28.70	28.95	25.17	29.75
	SSIM	0.880	0.890	0.904	0.903	0.905	0.914	0.912	0.866	0.917
	Time	0.015	91.493	4.047	1.167	287.476	37.932	10.566	652.745	7.074
Pepper	PSNR	29.06	29.43	30.03	29.93	29.95	30.16	30.39	26.65	30.48
	SSIM	0.764	0.772	0.779	0.779	0.779	0.781	0.786	0.732	0.788
	Time	0.011	58.071	2.850	0.881	190.785	17.517	8.407	404.304	5.232
PPT	PSNR	21.17	21.56	22.44	22.30	22.30	22.65	23.13	19.76	23.45
	SSIM	0.830	0.846	0.870	0.865	0.865	0.873	0.886	0.812	0.886
	Time	0.010	47.589	3.078	0.990	176.978	42.968	9.834	667.489	6.449
Zebra	PSNR	23.55	24.20	25.22	25.20	25.17	25.71	26.45	21.31	27.07
	SSIM	0.704	0.732	0.762	0.766	0.770	0.771	0.804	0.667	0.826
	Time	0.009	54.000	2.460	0.876	167.638	43.599	10.067	398.469	4.222
Bridge	PSNR	23.65	23.94	24.33	24.35	24.38	24.42	24.77	22.63	24.99
	SSIM	0.585	0.608	0.633	0.639	0.645	0.642	0.672	0.566	0.698
	Time	0.010	59.635	2.859	0.957	195.138	34.385	11.670	459.461	5.221
Man	PSNR	24.82	25.16	25.72	25.73	25.78	25.96	26.26	23.46	26.49
	SSIM	0.676	0.695	0.718	0.721	0.715	0.725	0.745	0.654	0.763
	Time	0.010	67.478	2.791	0.937	178.226	31.548	10.812	427.198	5.236
Average	PSNR	25.32	25.77	26.42	26.39	26.41	26.68	27.05	22.82	27.38
	SSIM	0.723	0.740	0.759	0.758	0.763	0.768	0.780	0.703	0.792
	Time	0.009	46.054	2.285	0.763	143.634	25.128	7.428	342.804	4.032

Zeyde’s method, demonstrating the superior efficiency for the proposed simple sigmoid transformation.

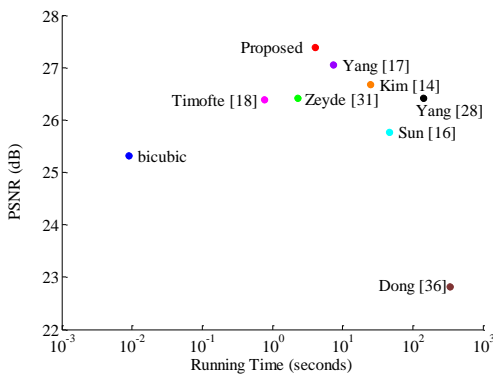


Fig. 14 Plot of the trade-off between accuracy and speed for ranged methods with upscaling factor 3. The results present the mean PSNR values and running time on the test images.

Overall, as shown in Fig. 14, our method realizes dominant reconstruction performance without much loss of efficiency, performing superior to Yang’s method known as state-of-the-art SISR approach with respect to PSNR value, and competitive to Zeyde’s methods concerning running time. As our method requires no training process, the superiority in efficiency can be more prominent if we take training time

into consideration.

C. Robustness

To further demonstrate the robustness of the proposed method to various Gaussian blurring kernels, upscaling factors and noise intensities, additional experiments are conducted on Set5 and Set14 datasets in this section, and the quantitative results are presented in Tables. IV-VI.

● Blurring kernel

Table. IV presents the comparison of reconstruction performance with various blurring kernels under the condition of upscaling factor 3. As we can see, the overall reconstruction performance for various methods degenerates with blurring kernel width increased. Under the condition of $\sigma = 0.8$, although Kim’s method performs superiorly with highest PSNR value in average, our method is still comparable and outperforms other approaches. Concerning conditions of $\sigma = 1.2$ and $\sigma = 1.6$, the proposed method outperforms other approaches in average while Yang’s method, as the most competitive one, also performs competitively when $\sigma = 1.6$. Overall, with blurring kernel width varying, the proposed method performs as the dominant one on most test images when $\sigma = 1.2$ and $\sigma = 1.6$, and achieves second best performance after Kim’s method when $\sigma = 0.8$, indicating

TABLE IV COMPARISON OF RECONSTRUCTION PERFORMANCE WITH VIROUS σ . THE BEST RESULTS ARE SHOWN IN BOLD.

	σ	Bicubic	Sun [16]	Zeyde [31]	Timofte [18]	Yang [28]	Kim [14]	Yang [17]	Dong [36]	Proposed
Baby	0.8	31.73	32.07	33.02	33.04	33.00	33.12	32.67	28.31	33.21
	1.2	30.91	31.47	32.12	32.11	32.11	32.22	32.86	28.32	33.22
	1.6	30.16	30.78	31.17	31.12	31.08	31.18	32.89	28.28	32.90
Bird	0.8	29.75	30.12	31.35	31.39	31.25	31.67	30.95	26.38	31.46
	1.2	28.72	29.29	30.06	30.06	30.00	30.29	30.89	26.26	31.19
	1.6	27.80	28.40	28.82	28.78	28.71	28.90	30.68	26.12	30.55
Butterfly	0.8	22.11	22.53	24.01	24.00	24.15	25.17	23.72	30.25	24.60
	1.2	21.33	21.95	22.93	22.86	22.96	23.76	23.88	20.23	24.75
	1.6	20.63	21.29	21.85	21.74	21.76	22.36	23.99	20.18	24.32
Head	0.8	29.82	29.97	30.37	30.43	30.40	30.53	30.19	28.06	30.42
	1.2	29.43	29.67	29.95	30.00	30.00	30.08	30.25	28.08	30.41
	1.6	29.06	29.32	29.49	29.51	29.51	29.55	30.19	28.04	30.24
Woman	0.8	26.49	26.87	28.37	28.39	28.43	28.75	28.03	23.46	28.66
	1.2	25.66	26.24	27.24	27.20	27.22	27.56	28.33	23.46	28.79
	1.6	24.93	25.53	26.13	26.06	26.02	26.30	28.55	23.41	28.36
Baboon	0.8	21.01	21.11	21.29	21.34	21.33	21.37	21.23	20.35	21.35
	1.2	20.75	20.89	21.03	21.08	21.09	21.13	21.24	20.37	21.32
	1.6	20.51	20.63	20.73	20.77	20.78	20.80	21.21	20.32	21.18
Barbara	0.8	24.44	24.59	25.00	24.98	25.02	24.94	24.83	22.85	25.12
	1.2	24.04	24.27	24.89	24.60	24.63	24.68	24.90	22.86	25.14
	1.6	23.67	23.90	24.13	24.14	24.14	24.24	25.00	22.83	24.95
Coastguard	0.8	25.00	25.18	25.62	25.55	25.63	25.65	25.54	23.93	25.68
	1.2	24.60	24.85	25.26	25.21	25.35	25.34	25.54	23.93	25.73
	1.6	24.23	24.46	24.78	24.73	24.87	24.84	25.52	23.88	25.55
Comic	0.8	21.27	21.49	22.11	22.20	22.24	22.39	21.95	19.71	22.34
	1.2	20.73	21.05	21.49	21.57	21.62	21.76	22.04	19.72	22.33
	1.6	20.24	20.55	20.85	20.88	20.90	21.01	22.05	19.67	22.02
Flowers	0.8	24.91	25.16	25.91	25.96	25.98	26.18	25.65	23.02	26.08
	1.2	24.25	24.62	25.15	25.18	25.21	25.35	25.68	22.96	25.98
	1.6	23.66	24.03	24.37	24.37	24.37	24.48	25.62	22.85	25.61
Foreman	0.8	29.00	29.41	30.88	30.98	30.84	31.69	30.59	27.12	31.06
	1.2	28.23	28.81	29.75	29.71	29.63	30.30	30.82	27.11	31.11
	1.6	27.55	28.13	28.61	28.59	28.49	28.93	30.61	26.99	30.65
Lena	0.8	29.44	29.71	30.57	30.63	30.61	30.88	30.40	26.43	30.60
	1.2	28.81	29.23	29.84	29.86	29.88	30.14	30.49	26.45	30.63
	1.6	28.24	28.68	29.07	29.04	29.04	29.23	30.48	26.43	30.37
Monarch	0.8	27.43	27.82	29.12	29.14	29.23	30.02	28.79	25.20	29.67
	1.2	26.63	27.22	28.07	28.04	28.10	28.70	28.95	25.14	29.75
	1.6	25.90	26.53	27.01	26.95	26.93	27.41	29.07	25.10	29.32
Pepper	0.8	29.65	29.87	30.68	30.59	30.60	30.85	30.50	26.72	30.62
	1.2	29.06	29.43	30.03	29.93	29.95	30.16	30.39	26.65	30.48
	1.6	28.50	28.92	29.31	29.20	29.17	29.37	30.10	26.55	30.19
PPT	0.8	21.78	22.03	23.21	23.07	23.09	23.59	23.10	19.82	23.39
	1.2	21.17	21.56	22.44	22.30	22.30	22.65	23.13	19.76	23.45
	1.6	20.59	21.01	21.60	21.47	21.39	21.68	23.27	19.72	23.09
Zebra	0.8	24.49	24.92	26.47	26.47	26.44	27.02	26.18	21.35	26.93
	1.2	23.55	24.20	25.22	25.20	25.17	25.71	26.45	21.31	27.07
	1.6	22.71	23.39	23.99	23.94	23.88	24.30	26.70	21.28	26.57
Bridge	0.8	24.10	24.29	24.80	24.81	24.82	24.88	24.62	22.62	24.94
	1.2	23.65	23.94	24.33	24.35	24.38	24.42	24.77	22.63	24.99
	1.6	23.22	23.52	23.78	23.79	23.79	23.85	24.85	22.61	24.80
Man	0.8	25.32	25.54	26.29	26.33	26.35	26.60	26.10	23.45	26.43
	1.2	24.82	25.16	25.72	25.73	25.78	25.96	26.26	23.46	26.49
	1.6	24.36	24.71	25.09	25.06	25.07	25.22	26.36	23.46	26.27
Average	0.8	25.99	26.26	27.17	27.18	27.19	27.52	26.95	24.39	27.36
	1.2	25.35	25.77	26.42	26.39	26.41	26.68	27.05	23.82	27.38
	1.6	24.78	25.21	25.60	25.56	25.55	25.76	27.06	23.76	27.06

strong robustness to ranged blurring kernels.

- Upscaling factor

In **Table V**, results concerning various upscaling factors are exhibited. Although mutual degeneration trend can be observed with upscaling factor increased from 2 to 4, our method still outperforms other state-of-the-art approaches in average with highest PSNR values, while Kim's method and

Yang's method perform superior to ours on several images under conditions of upscaling factor 2 and 4 respectively. On the whole, our method performs independent to exemplars and realize state-of-the-art and even better performance for range upscaling factors, demonstrating the superior robustness to upscaling factors.

TABLE V COMPARISON OF RECONSTRUCTION PERFORMANCE WITH VIROUS k . THE BEST RESULTS ARE SHOWN IN BOLD.

	k	Bicubic	Sun [16]	Zeyde [31]	Timofte [18]	Yang [28]	Kim [14]	Yang [17]	Dong [36]	Proposed
Baby	2	32.28	33.17	33.06	33.06	33.06	33.21	35.45	32.21	35.72
	3	30.91	31.47	32.12	32.11	32.11	32.22	32.86	28.32	33.22
	4	29.54	29.80	30.89	30.85	30.66	31.04	30.79	26.16	31.24
Bird	2	30.33	31.31	31.31	31.25	31.20	31.49	34.35	30.38	34.46
	3	28.72	29.29	30.06	30.06	30.00	30.29	30.89	26.26	31.19
	4	27.18	27.43	28.43	28.51	28.38	28.63	28.37	23.88	28.86
Butterfly	2	22.67	23.68	23.94	23.73	23.71	24.10	28.06	24.13	28.17
	3	21.33	21.95	22.93	22.86	22.96	23.76	23.88	20.23	24.75
	4	20.09	20.41	21.62	21.58	21.66	22.40	21.56	18.29	22.54
Head	2	30.15	30.47	30.52	30.53	30.55	30.56	31.34	30.23	31.57
	3	29.43	29.67	29.95	30.00	30.00	30.08	30.25	28.08	30.41
	4	28.72	28.85	29.25	29.29	29.25	29.37	29.20	26.68	29.42
Woman	2	27.11	28.03	28.19	28.13	28.07	28.35	32.08	27.47	32.06
	3	25.66	26.24	27.24	27.20	27.22	27.56	28.33	23.46	28.79
	4	24.37	24.64	25.84	25.80	25.71	26.24	25.82	21.53	26.43
Baboon	2	21.35	21.54	21.67	21.70	21.72	21.76	22.69	21.88	22.64

	3	20.75	20.89	21.03	21.08	21.09	21.13	21.24	20.37	21.32
	4	20.28	20.33	20.49	20.52	20.52	20.54	20.48	19.68	20.57
Barbara	2	24.80	25.10	25.26	25.23	25.25	25.33	26.48	25.12	26.48
	3	24.04	24.27	24.89	24.60	24.63	24.68	24.90	22.86	25.14
	4	23.33	23.44	23.79	23.82	23.80	23.98	23.79	21.69	24.00
Coastguard	2	25.53	25.94	26.32	26.32	26.40	26.45	28.47	26.51	28.61
	3	24.60	24.85	25.26	25.21	25.35	25.34	25.54	23.93	25.73
	4	23.92	24.03	24.30	24.32	24.25	24.38	24.36	22.99	24.50
Comic	2	21.84	22.35	22.60	22.61	22.62	22.76	25.13	22.83	25.21
	3	20.73	21.05	21.49	21.57	21.62	21.76	22.04	19.72	22.33
	4	19.81	19.94	20.44	20.47	20.47	20.56	20.43	18.27	20.74
Flowers	2	25.52	26.11	26.28	26.24	26.25	26.39	28.45	26.16	28.50
	3	24.25	24.62	25.15	25.18	25.21	25.35	25.68	22.96	25.98
	4	23.17	23.35	23.96	24.01	23.98	24.16	23.91	21.31	24.30
Foreman	2	29.32	30.25	30.40	30.24	30.24	30.48	32.37	30.32	33.66
	3	28.23	28.81	29.75	29.71	29.63	30.30	30.82	27.11	31.11
	4	27.22	27.51	28.74	28.67	28.52	29.35	28.06	25.38	29.15
Lena	2	29.91	30.48	30.62	30.60	30.58	30.75	32.50	29.73	32.54
	3	28.81	29.23	29.84	29.86	29.88	30.14	30.49	26.45	30.63
	4	27.78	27.99	28.76	28.83	28.70	29.11	28.81	24.66	29.02
Monarch	2	28.03	29.00	29.18	29.04	29.02	29.38	32.93	29.11	33.13
	3	26.63	27.22	28.07	28.04	28.10	28.70	28.95	25.14	29.75
	4	25.35	25.64	26.68	26.71	26.77	27.25	26.62	23.13	27.54
Pepper	2	30.02	30.54	30.65	30.57	30.58	30.74	31.49	29.50	31.76
	3	29.06	29.43	30.03	29.93	29.95	30.16	30.39	26.65	30.48
	4	28.04	28.23	29.06	28.99	28.79	29.25	29.00	24.75	29.19
PPT	2	22.50	23.18	23.61	23.44	23.47	23.73	26.79	23.42	26.81
	3	21.17	21.56	22.44	22.30	22.30	22.65	23.13	19.76	23.45
	4	19.98	20.14	21.01	20.86	20.73	21.24	21.00	18.20	21.35
Zebra	2	25.13	26.23	26.37	26.27	26.23	26.49	30.82	25.58	31.07
	3	23.55	24.20	25.22	25.20	25.17	25.71	26.45	21.31	27.07
	4	21.94	22.22	23.43	23.48	23.43	23.98	23.33	19.27	24.06
Bridge	2	24.54	24.97	25.18	25.17	25.20	25.27	27.12	25.18	27.13
	3	23.65	23.94	24.33	24.35	24.38	24.42	24.77	22.63	24.99
	4	22.80	22.93	23.39	23.39	23.37	23.38	23.35	21.39	23.60
Man	2	25.80	26.29	26.51	26.50	26.49	26.64	28.60	26.36	28.59
	3	24.82	25.16	25.72	25.73	25.78	25.96	26.26	23.46	26.49
	4	23.95	24.11	24.79	24.78	24.77	25.00	24.73	21.93	25.06
Average	2	26.49	27.15	27.32	27.26	27.26	27.44	29.73	27.01	29.90
	3	25.35	25.77	26.42	26.39	26.41	26.68	27.05	23.82	27.38
	4	24.308	24.50	25.27	25.27	25.21	25.55	25.20	22.18	25.64

● Noise intensity

Table VI shows the reconstruction performance with various noise intensities. As analyzed in Section II, the patch-wise slope-based implementation of our method performs innate suppression of noise, which can be demonstrated

by the superior performance with highest PSNR in average. Although sparsity-deduced approaches like Kim’s and Yang’s methods have advantages in noise suppression, our method still outperforms them except for several conditions where our method performs slightly inferior.

TABLE VI COMPARISON OF RECONSTRUCTION PERFORMANCE WITH VIROUS NOISE INTENSITIES. THE BEST RESULTS ARE SHOWN IN BOLD.

	σ_N	Bicubic	Sun [16]	Zeyde [31]	Timofte [18]	Yang [28]	Kim [14]	Yang [17]	Dong [36]	Proposed
Baby	0	30.91	31.47	32.12	32.11	32.11	32.22	32.86	28.32	33.22
	2	30.78	31.32	31.93	31.91	31.89	32.02	32.57	28.23	32.76
	4	30.43	30.90	31.42	31.37	31.30	31.48	31.87	27.94	31.71
Bird	0	28.72	29.29	30.06	30.06	30.00	30.29	30.89	26.26	31.19
	2	28.64	29.19	29.91	29.91	29.84	30.14	30.67	26.18	30.88
	4	28.43	28.93	29.61	29.57	29.47	29.77	30.14	25.98	30.15
Butterfly	0	21.33	21.95	22.93	22.86	22.96	23.76	23.88	20.23	24.75
	2	21.32	21.93	22.91	22.83	22.94	23.72	23.83	20.19	24.68
	4	21.28	21.88	22.85	22.76	22.86	23.62	23.73	20.14	24.49
Head	0	29.43	29.67	29.95	30.00	30.00	30.08	30.25	28.08	30.41
	2	29.33	29.56	29.83	29.86	29.85	29.96	30.07	27.91	30.13
	4	29.07	29.27	29.47	29.48	29.44	29.59	29.59	27.55	29.44
Woman	0	25.66	26.24	27.24	27.20	27.22	27.56	28.33	23.46	28.79
	2	25.63	26.20	27.19	27.14	27.16	27.50	28.22	23.40	28.62
	4	25.51	26.05	26.99	26.95	26.93	27.27	27.90	23.30	28.14
Baboon	0	20.75	20.89	21.03	21.08	21.09	21.13	21.24	20.37	21.32
	2	20.74	20.87	21.01	21.06	21.08	21.11	21.22	20.34	21.29
	4	20.71	20.83	20.97	21.01	21.02	21.06	21.15	20.29	21.20
Barbara	0	24.04	24.27	24.89	24.60	24.63	24.68	24.90	22.86	25.14
	2	24.01	24.24	24.55	24.56	24.59	24.65	24.85	22.83	25.07
	4	23.94	24.16	24.45	24.46	24.48	24.54	24.71	22.73	24.85
Coastguard	0	24.60	24.85	25.26	25.21	25.35	25.34	25.54	23.93	25.73
	2	24.58	24.83	25.22	25.17	25.31	25.30	25.49	23.88	25.63
	4	24.48	24.72	25.09	25.03	25.15	25.17	25.31	23.78	25.38
Comic	0	20.73	21.05	21.49	21.57	21.62	21.76	22.04	19.72	22.33
	2	20.72	21.03	21.47	21.54	21.60	21.73	22.01	19.70	22.29
	4	20.68	20.99	21.42	21.49	21.54	21.67	21.92	19.67	22.18
Flowers	0	24.25	24.62	25.15	25.18	25.21	25.35	25.68	22.96	25.98
	2	24.22	24.59	25.11	25.13	25.17	25.31	25.62	22.93	25.89
	4	24.14	24.49	25.00	25.01	25.03	25.18	25.45	22.83	25.64
Foreman	0	28.23	28.81	29.75	29.71	29.63	30.30	30.82	27.11	31.11
	2	28.17	28.73	29.65	29.60	29.52	30.17	30.62	27.03	30.81
	4	27.99	28.51	29.35	29.29	29.17	29.81	30.12	26.81	30.07
Lena	0	28.81	29.23	29.84	29.86	29.88	30.14	30.49	26.45	30.63
	2	28.73	29.14	29.72	29.73	29.75	30.01	30.32	26.36	30.36
	4	28.50	28.87	29.39	29.38	29.36	29.65	29.86	26.16	29.68
Monarch	0	26.63	27.22	28.07	28.04	28.10	28.70	28.95	25.14	29.75

	2	26.58	27.16	27.98	27.95	28.00	28.61	28.84	25.12	29.53
	4	26.44	26.99	27.76	27.72	27.74	28.35	28.52	24.96	28.96
Pepper	0	29.06	29.43	30.03	29.93	29.95	30.16	30.39	26.65	30.48
	2	28.98	29.33	29.92	29.81	29.81	30.04	30.23	26.57	30.22
	4	28.73	29.04	29.56	29.44	29.40	29.67	29.76	26.35	29.53
	0	21.17	21.56	22.44	22.30	22.30	22.65	23.13	19.76	23.45
PPT	2	21.16	21.56	22.43	22.29	22.29	22.65	23.11	19.75	23.41
	4	21.13	21.53	22.39	22.25	22.24	22.61	23.06	19.73	23.33
	0	23.55	24.20	25.22	25.20	25.17	25.71	26.45	21.31	27.07
Zebra	2	23.52	24.18	25.18	25.15	25.13	25.66	26.37	21.29	26.95
	4	23.45	24.09	25.05	25.03	24.99	25.50	26.15	21.22	26.62
	0	23.65	23.94	24.33	24.35	24.38	24.42	24.77	22.63	24.99
Bridge	2	23.62	23.91	24.29	24.31	24.34	24.40	24.71	22.61	24.92
	4	23.55	23.83	24.19	24.20	24.22	24.29	24.56	22.52	24.71
	0	24.82	25.16	25.72	25.73	25.78	25.96	26.26	23.46	26.49
Man	2	24.78	25.12	25.66	25.66	25.71	25.92	26.18	23.43	26.38
	4	24.70	25.01	25.54	25.53	25.56	25.77	25.99	23.30	26.11
	0	25.35	25.77	26.42	26.39	26.41	26.68	27.05	23.82	27.38
Average	2	25.31	25.72	26.33	26.31	26.33	26.61	26.94	23.76	27.21
	4	25.18	25.56	26.14	26.11	26.11	26.39	26.66	23.63	26.79

V. CONCLUSIONS AND FUTURE WORK

In this paper, we propose a fast and simple single image super-resolution algorithm based on sigmoid transformation, utilize the overlapped patch-wise sigmoid transformation to realize slope-based sharpening of the image, and implement the sharpening operation as an imposed sharpening regularization term in the reconstruction. Extensive experiments compared with other state-of-the-art approaches demonstrate the superiority of the proposed algorithm in effectiveness and efficiency. Considering the fast, simple and effective SR processing of the proposed method with no need for learning or training, it has widespread application value and prospect.

Although the proposed overlapped patch-wise sigmoid transformation realizes state-of-the-art and even better reconstruction performance, the parameters utilized including steepest parameter K and location parameter B are empirically determined, which can be further improved. In the future, we will investigate the adaptive determination of the parameters to enhance the adaptability of sigmoid transformation to complex images.

REFERENCES

- [1] V. Chandran, C. Fookes, F. Lin, S. Sridharan, "Investigation into optical flow super-resolution for surveillance applications," *Aprs Workshop on Digital Image Computing*, vol. 26, no. 47, pp. 73–78, 2005.
- [2] L. Zhang, H. Zhang, H. Shen, and P. Li, "A super-resolution reconstruction algorithm for surveillance images," *Signal Processing*, vol. 90, no. 3, pp. 848–859, 2010.
- [3] A. J. Tatem, H. G. Lewis, P.M. Atkinson, M.S. Nixon, "Super-resolution target identification from remotely sensed images using a hopfield neural network," *IEEE Trans. Geosci. Rem. Sens.*, vol. 39, no. 4, pp. 781–796, Apr. 2001.
- [4] M. W. Thornton, P. M. Atkinson, and D. a. Holland, "Sub-pixel mapping of rural land cover objects from fine spatial resolution satellite sensor imagery using super-resolution pixel-swapping," *International Journal of Remote Sensing*, vol. 27, no. 3, pp. 473–491, Jan. 2006.
- [5] K. Makantasis, K. Karantzas, A. Doulmis, N. Doulamis, "Deep supervised learning for hyperspectral data classification through convolutional neural networks," in *Proc. IGARSS*, Jul. 2015, pp. 4959–4962.
- [6] H. Greenspan, G. Oz, N. Kiryati, S. Peled, "Super-resolution in MRI," in *Proc. ISBI*, 2002, pp. 943–946.
- [7] W. Shi, J. Caballero, C. Ledig, X. Zhuang, W. Bai, K. Bhatia, A. Marva, T. Dawes, D. O'Regan, and D. Rueckert, "Cardiac image super-resolution with global correspondence using multi-atlas patchmatch," in *Proc. Int. Conf. Medical Image Computing and Computer Assisted Intervention (MICCAI)*, Jan. 2013, pp. 9–16.
- [8] T. Goto, T. Fukuoka, F. Nagashima, S. Hirano and M. Sakurai, "Super-resolution system for 4K-HDTV," in *Proc. Int Conf. Pattern Recognition*, Jan. 2014, pp. 4453–4458.
- [9] K. Zhang, X. Gao, D. Tao and X. Li, "Multi-scale dictionary for single image super-resolution," in *Proc. CVPR*, Providence, RI, Jun. 2012, pp. 1114–1121.
- [10] M. Irani and S. Peleg. "Improving resolution by image registration." *Graphical Models and Image Processing*, vol. 53, no. 3, pp. 231–239, 1991.
- [11] R. Fattal. "Image upsampling via imposed edge statistics," *ACM SIG-GRAPH*, vol. 26, no. 3, pp. 95, 2007.
- [12] S. C. Park, M. K. Park and M. G. Kang, "Super-resolution image reconstruction: A technical overview," *IEEE Signal Processing Magazine*, vol. 20, no. 3, pp. 21–36, May. 2003.
- [13] J. Sun, et al. "Image super-resolution using gradient profile prior," in *Proc. IEEE Comput. Soc. Conf. Comput. Vis. Pattern Recognit.*, 2008, pp. 1–8.
- [14] K. I. Kim and Y. Kwon. "Single-image super-resolution using sparse regression and natural image prior," *IEEE Trans. Pattern Anal. Mach. Intell.*, vol. 32, no. 6, pp. 1127–1133, 2010.
- [15] G. Freedman and R. Fattal. "Image and video upscaling from local self-examples," *ACM Trans. Graph.*, vol. 30, no. 2, pp. 1–11, 2011.
- [16] J. Sun, et al. "Gradient profile prior and its applications in image super-resolution and enhancement," *IEEE Trans. Image Process.*, vol. 20, no. 6, pp. 1529–1542, 2011.
- [17] C. Yang, and M. H. Yang. "Fast direct super-resolution by simple functions," in *Proc. ICCV*, 2013, pp. 561–568.
- [18] R. Timofte, V. De, and L. V. Gool. "Anchored neighborhood regression for fast example-based super-resolution," in *Proc. ICCV*, 2014, pp. 1920–1927.
- [19] C. Yang, C. Ma, and M. H. Yang. "Single-image super-resolution: A benchmark," in *Proc. ECCV*, 2014, pp. 372–386.
- [20] Z. Zhu, et al. "Fast single image super-resolution via self-example learning and sparse representation," *IEEE Trans. Multimedia* 16.8(2014):2178–2190.
- [21] S. Gu, et al. "Convolutional sparse coding for image super-resolution," in *Proc. ICCV*, 2016, pp. 1823–1831.
- [22] X. Gao, K. Zhang, D. Tao and X. Li, "Image super-resolution with sparse neighbor embedding," *IEEE Trans. Image Process.*, vol. 21, no. 7, pp. 3194–3205, Jul. 2012.
- [23] L. Zhang and X. Wu, "An edge-guided image interpolation algorithm via directional filtering and data fusion," *IEEE Trans. Image Process.*, vol. 15, no. 8, pp. 2226–2238, Aug. 2006.
- [24] H. A. Aly and E. Dubois. "Image up-sampling using total variation regularization with a new observation model," *IEEE Trans. Image Process.*, vol. 14, no. 10, pp. 1647–1659, 2005.
- [25] S. Dai, M. Han, W. Xu, Y. Wu, and Y. Gong. "Soft edge smoothness prior for alpha channel super resolution," in *Proc. CVPR*, Minneapolis, MN, Jun. 2007, pp. 1–8.
- [26] H. S. Hou and H. C. Andrews. "Cubic splines for image interpolation and digital filtering," *IEEE Trans. Acoustics, Speech & Signal Proc.*, ASSP-26:508–517. 449
- [27] W. Liu, S. Li, "Sparse representation with morphologic regularizations for single image super-resolution," *Signal Processing*, vol. 98, pp. 410–422, 2014.
- [28] J. Yang, J. Wright, T. Huang. "Image super-resolution as sparse representation of raw image patches," *IEEE Trans. Image Process.*, vol. 19, no. 11, pp. 2861,2010.
- [29] Q. He, C. Zhang, D. C. Liu. "Nonlinear image enhancement by self-adaptive sigmoid function," *International Journal of Signal Processing, Image Processing and Pattern Recognition*, vol. 8, no. 11, pp. 319–328, 2015.
- [30] E. F. Arriaga-Garcia, R. E. Sanchez-Yanez, M. G. Garcia-Hernandez,

- “Image enhancement using Bi-histogram equalization with adaptive sigmoid functions,” in *Proc. International Conference on Electronics, Communications and Computers (CONIELECOMP)*, 2014, pp. 28-34.
- [31] R. Zeyde, M. Elad, and M. Protter. “On single image scale-up using sparse-representations,” in *Proc. International Conference on Curves and Surfaces*, 2010, pp. 711–730.
- [32] D. Glasner, S. Bagon, M. Irani. “Super-resolution from a single image,” in *Proc. ICCV*, 2009, pp.349-356
- [33] C. Dong, C. C. Loy, K. He and X. Tang, “Learning a deep convolutional network for image super-resolution,” In *Proc. ECCV*, 2014, pp. 184-199.
- [34] L. He, H. Qi and R. Zaretzki, “Beta process joint dictionary learning for coupled feature spaces with application to single image super-resolution,” In *Proc. CVPR*, 2013, pp. 345-352.
- [35] M. T. Merino and J. Nunez, “Super-resolution of remotely sensed images with variable-pixel linear reconstruction,” *IEEE Trans. Geosci. Rem. Sens.*, vol. 45, no. 5, pp. 1446-1457, May. 2007.
- [36] W. Dong, L. Zhang, G. Shi, X. Wu, “Image deblurring and super-resolution by adaptive sparse domain selection and adaptive regularization,” *IEEE Trans. Image Process.*, vol. 20, no. 7, pp. 1838-1857, 2011.
- [37] L. Wang, Z. Lin, X. Deng and W. An, “Multi-frame image super resolution with fast upscaling technique,” *arXiv preprint arXiv:1706.06266*, 2017.